Author/s:
Prabhakar, AT;Roy, A;Margabandhu, K;McKendrick, AM;Carter, O;Garrido, MI

Title:
Double dissociation of dynamic and static face perception provides causal evidence for a third visual pathway

Date:
2025-12-01

Citation:
Prabhakar, A. T., Roy, A., Margabandhu, K., McKendrick, A. M., Carter, O. & Garrido, M. I. (2025). Double dissociation of dynamic and static face perception provides causal evidence for a third visual pathway. Nature Communications, 16 (1), pp.6513-. https://doi.org/10.1038/s41467-025-61395-9.

Persistent Link:
https://hdl.handle.net/11343/363368

nature communications

Article

https://doi.org/10.1038/s41467-025-61395-9

Double dissociation of dynamic and static face perception provides causal evidence for a third visual pathway

Received: 13 September 2024

Accepted: 13 June 2025

Published online: 15 July 2025

Check for updates

A. T. Prabhakar[1,2] ✉, Anupama Roy[1], Kavitha Margabandhu[1], Allison M. McKendrick[3,4,5], Olivia Carter[2] & Marta I. Garrido[2,6]

The two-pathway ventral ("what") and dorsal ("where") model of visual perception has dominated neuroscience for over 30 years. In this framework, face perception, crucial for social interactions, is linked to the ventral pathway, which processes static features. However, dynamic facial expressions activate the superior temporal sulcus, outside both established pathways. An alternative model recently proposed a third visual pathway dedicated to dynamic facial expressions. Using neuroimaging and behavioral testing in 108 patients with focal brain lesions, we provide causal evidence of a double dissociation between static and dynamic face perception. Our findings show direct causal evidence for the putative third visual pathway that bypasses the occipital and fusiform face areas.

In the ambiance of a quaint café, a captivating moment unfolds as you engage in a silent dialogue with your companion across the table. With each subtle shift in their facial expression, a symphony of emotions fills you, effortlessly communicated without a single spoken word. Beneath the surface of this subtle exchange lies a sophisticated brain network, orchestrating the seamless communication of emotions via visual perception. The traditional two-pathway model of visual perception has long dominated neuroscience, delineating a ventral pathway for visual perception and a dorsal pathway for action (Fig. 1)[1–4]. Studies in humans and non-human primates have shown that the ventral visual pathway, which includes key functional areas such as the Occipital Face Area (OFA) and the Fusiform Face Area (FFA), is responsible for processing static aspects of face perception, such as facial identity and emotion recognition[1,4–6]. However, the recognition of dynamic facial expressions, biological motion (movement patterns characteristic of humans and animals), and social perception (interpretation of social cues from others) engages the posterior Superior Temporal Sulcus (pSTS), a region that is not a part of either the ventral or the dorsal pathway[7–9]. Research over the last few decades suggests the existence of a pathway along the lateral surface of the brain, distinct from the traditional dorsal and ventral pathways[10–16]. Regions such as the pSTS and others along the STS may be part of this pathway, contributing to face perception and social cognition (Fig. 1-blue)[14,16]. This putative *third pathway* is proposed to selectively respond to moving aspects of the face, biological motion, and social perception[14,16]. However, the precise causal roles of these regions, their structural and functional connectivity, their role in complex motion processing, and how they interact with other regions involved in face and body processing is still being elucidated[10,11,16–18]. Hence, demonstration of a double dissociation in human participants would provide important convergent evidence supporting the third visual pathway. Whilst a transcranial magnetic stimulation (TMS) study showed evidence for a transient double dissociation between dynamic and static emotion recognition when inhibiting pSTS[19], here we ask whether such dissociation persists in patients with the relevant focal lesions.

Although functional neuroimaging and non-human primate studies have provided significant insights into face perception, large human lesion-based studies have been limited[5,8,19–21]. Human lesion studies have the advantage of providing strong causal evidence rather than mere correlational associations[22]. Here we directly tested the existence of the putative third visual pathway by assessing facial emotion recognition in 108 patients with focal lesions in the occipital,

[1]Cognitive Neuroscience and Clinical Phenomenology Laboratory, Department of Neurological Sciences, Christian Medical College, Vellore, India. [2]Melbourne School of Psychological Sciences, University of Melbourne, Melbourne, VIC, Australia. [3]Division of Optometry, School of Allied Health, University of Western Australia, Melbourne, VIC, Australia. [4]Lions Eye Institute, Perth, WA, Australia. [5]Department of Optometry & Vision Sciences, University of Melbourne, Melbourne, VIC, Australia. [6]Graeme Clark Institute for Biomedical Engineering, Melbourne, VIC, Australia. ✉e-mail: atprabhakar@gmail.com

https://doi.org/10.1038/s41467-025-61395-9

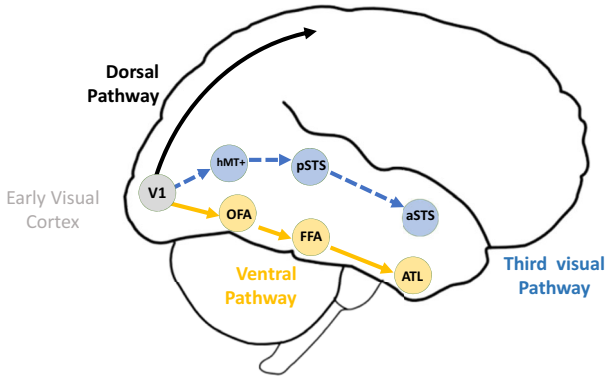

Fig. 1 | Cortical visual pathways in the human brain. Schematic representation of the three cortical visual pathways in the human brain. The dorsal pathway (black), ventral pathway (Yellow), and putative third Visual Pathway (blue dotted line) originate in the primary Visual Cortex (V1) and extend to various specialized visual regions. The ventral pathway, also known as the "what" pathway, is involved in object recognition and static aspects of face perception. It links V1 to the Occipital Face Area (OFA)/ IOG-faces, and the Fusiform Face Area (FFA), and then extends to the anterior temporal lobe face regions (ATL). The OFA is a cluster along the inferior occipital gyrus (IOG), while the FFA area consists of two subregions pFus-faces/FFA1 and mFus-faces/FFA-2 along the fusiform gyrus. The dorsal pathway, also known as the "where" pathway, is involved in vision for action and spatial relationships and projects to the parietal lobe. The putative third pathway originates in the primary visual cortex (V1) and extends to the motion-selective area hMT+. It then proceeds to the posterior banks of the superior temporal sulcus (pSTS), continues to the anterior superior temporal sulcus (aSTS), and finally projects to the anterior temporal lobe.

parietal, and temporal lobes. We hypothesized that if the static aspects of facial recognition are part of the ventral pathway and the dynamic aspects of facial perception are part of the putative third pathway that projects to the pSTS, there should be a double dissociation between dynamic and static facial recognition.

All patients underwent detailed neurological examination and a battery of behavioral tasks to assess visual function (see "Methods"). To assess static emotion recognition, we used color photographs of faces of different ethnicities. Participants had to choose from the displayed options (5AFC: happy, sad, fearful, angry, or neutral) with a verbal response. To assess dynamic emotion recognition, we played 1.5-s video clips of emotional expressions and participants were asked to choose from the displayed options (6AFC: happy, sad, fearful, angry, surprised, or disgust) with a verbal response. Each patient's brain lesion was identified based on their individual magnetic resonance images and manually mapped to the MNI template brain. Statistical associations between lesion location and behavioral performance were then investigated.

Results

Double dissociation between static and dynamic emotion recognition

To look for a double dissociation between performance on dynamic and static emotion recognition and its association with lesion location, we first conducted a region of interest (ROI) analysis. As the face processing network is known to be right lateralized, we used FFA (MNI coordinates: 40, −55, −12), OFA (MNI coordinates: 39, −79, −6) and pSTS (MNI coordinates: 50, −47, 13) in the right hemisphere as regions of interest[23]. We categorized patients based on whether their lesion overlapped within these ROIs and compared their performance accuracy on the static and dynamic facial expression recognition tasks. Each patient's lesion map in MNI space was overlayed with the selected ROIs to determine their overlap (Table S4). Patients were then categorized into four lesion groups: (1) right pSTS only ($N = 31$), (2) right OFA/FFA only ($N = 12$), (3) both right pSTS and OFA/FFA ($N = 15$), and (4) neither involved ($N = 50$). A GLM analyzed main effects and interactions, with static and dynamic emotion recognition accuracies alternately as dependent variables and lesion groups as the independent factor. We found a significant main effect of lesion location on static emotion recognition (F (3103) = 22.1, $p < 0.001$, $\eta^2p = 0.392$, 95% CI [0.241, 0.506]), and on dynamic emotion recognition (F (3103) = 12.5, $p < 0.001$, $\eta^2p = 0.266$, 95% CI [0.121, 0.389]). Post-hoc tests revealed that the right FFA/OFA lesioned group ($N = 12$) had significantly lower performance on static emotion recognition (t (103) = 6.29, $p < 0.001$) compared to the right pSTS lesioned group ($N = 31$) (Figs. 2A, B and 3). In contrast, the right pSTS lesioned group had significantly lower accuracy on dynamic emotion recognition compared to FFA/OFA lesioned group (t (103) = 5.61, $p < 0.001$), thus demonstrating a double dissociation (Figs. 2A, B and 3). We repeated a similar analysis using the left FFA(MNI coordinates: −38, −58, −14), OFA (MNI coordinates: −41, −81, −4), and left pSTS (MNI coordinates: −50, −48, 15) ROIs[23]. Our results did not show a significant effect of the left FFA/OFA lesions ($N = 9$) on the performance of static emotion recognition (F (3103) = 0.63, $p = 0.600$, $\eta^2p = 0.018$, 95% CI [0, 0.071]) (Fig. 4). However, isolated lesions of left pSTS ($N = 9$) were associated with lower scores on dynamic emotions recognition (F (3103) = 3.61, $p = 0.016$, $\eta^2p = 0.095$, 95% CI [0.003, 0.199]). We also found that pulvinar lesions ($N = 5$, left = 3, right = 2) were associated with poor performance on dynamic emotion recognition (F (1105) = 14.08, $p < 0.001$, $\eta^2p = 0.118$, 95% CI [0.027, 0.241]), despite intact pSTS. Thus, we were able to demonstrate a double dissociation between static and dynamic emotion recognition, with right hemispheric lesions involving the FFA/OFA impairing static recognition and pSTS lesions impairing dynamic recognition. Though left sided lesions involving the FFA/OFA had no significant effect on static recognition, left pSTS lesions and pulvinar lesions sparing pSTS were associated with impaired dynamic emotion recognition.

Dissociation between dynamic face processing and global visual motion perception

We asked whether impaired dynamic emotion recognition might stem from a broader deficit in global motion perception. To answer that question, we computed the correlation between the behavioural scores of dynamic emotion recognition and motion direction discrimination, but found no evidence for a correlation (Pearson's $r = 0.16$, $p = 0.106$). To further rule out the possibility of a global motion perception deficit, we then asked if the involvement of V5/hMT + (a key region associated with global visual motion perception) by the lesion had any association with performance on the dynamic emotion recognition task. Patients were categorized as follows: isolated unilateral pSTS lesions ($N = 23$), isolated unilateral hMT+ lesions ($N = 5$), bilateral hMT+ lesions ($N = 1$), bilateral hMT+ lesions with pSTS involvement ($N = 2$), unilateral hMT+ and pSTS involvement ($N = 19$), and no involvement of pSTS or hMT+ ($N = 58$). We found that patients with isolated pSTS lesions had normal scores on motion direction discrimination but significantly lower scores on dynamic emotion recognition compared to patients with isolated hMT+ lesions (t (97) = 3.312, $p_{\text{Bonferroni}} = 0.002$) (Fig. 5). Conversely, one patient, who had a bilateral hMT+ lesion with sparing of the pSTS had normal performance on the dynamic facial recognition task but severely impaired motion discrimination, demonstrating a double dissociation between motion direction discrimination and dynamic emotion recognition (Crawford's $p < 0.001$) (Fig. 5), and suggesting a short-cut for dynamic emotion recognition with visual inputs to pSTS bypassing hMT+.

Multivariate lesion symptom mapping using support vector regression

In order to complement the findings of the ROI-based analysis, we performed a support vector regression lesion symptom mapping (SVR-LSM), which provides an apriori, voxel-wise, multivariate view

https://doi.org/10.1038/s41467-025-61395-9

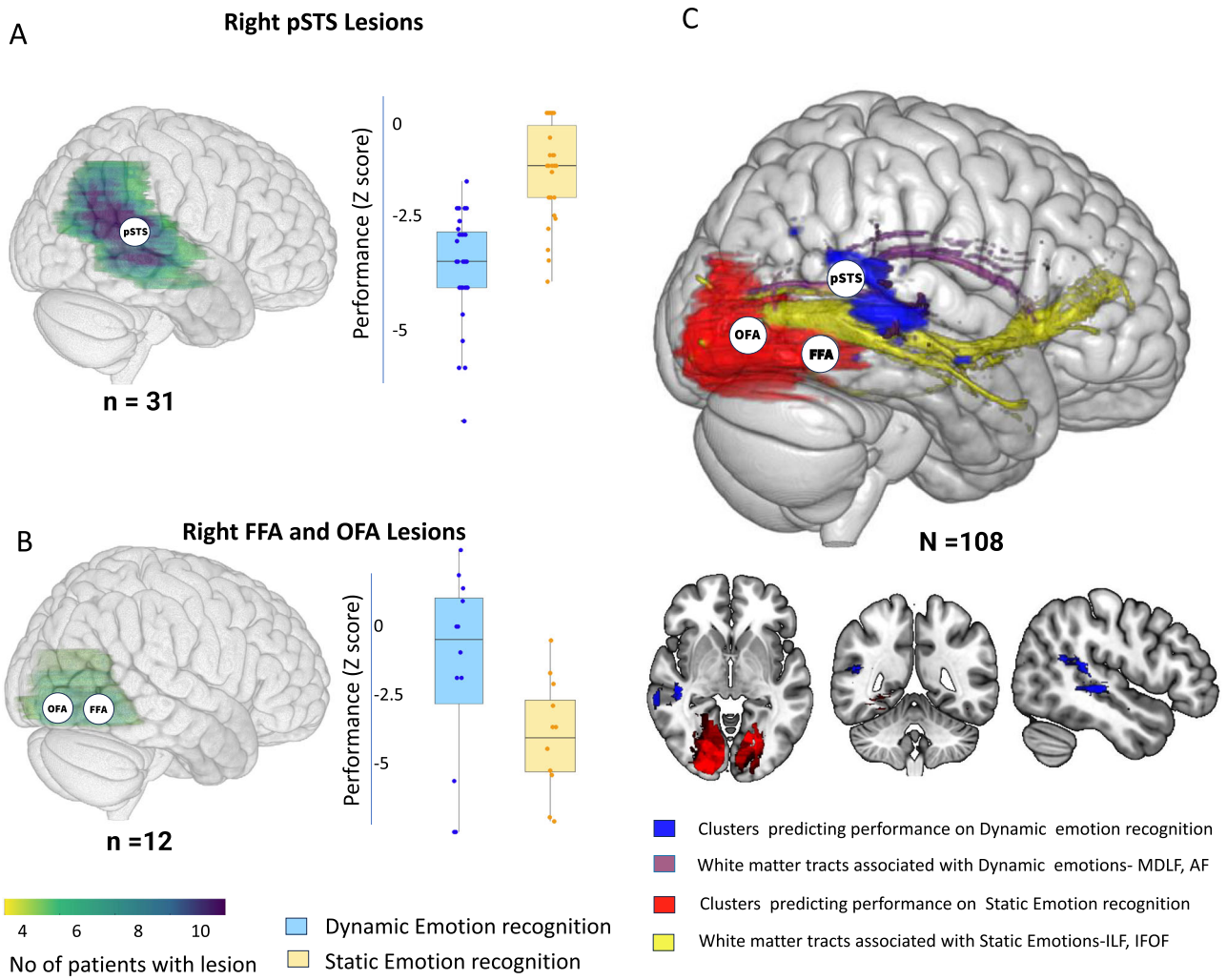

Fig. 2 | Double dissociation between dynamic and static emotion recognition. Performance on static and dynamic emotion recognition tasks and brain lesion mapping in patients with focal brain lesions (**A**) 31 Patients with focal brain lesions involving the right posterior superior temporal sulcus (pSTS) but sparing the right fusiform face area (FFA) and occipital face area (OFA), showed normal performance in the static emotion recognition task but poor performance for dynamic emotion recognition. **B** 12 patients with focal brain lesions involving the right FFA or OFA, but sparing the right pSTS, showed normal performance in dynamic but poor performance in static emotion recognition. In (**A**, **B**), the rendered MNI152 template brain shows the extent of the associated lesions in green. The boxplots show the z-transformed performance accuracy of the static and dynamic emotion recognition tasks. The boxes denote the interquartile range, the whiskers extend to 1.5 × IQR from each quartile and the horizontal lines denote the median. The source data and code used for generating the plots are available at https://osf.io/ez9dp/. **C** Rendered MNI152 template brain and orthogonal brain slices show results of the multivariate support vector regression lesion symptom mapping (SVR-LSM). Clusters show significant associations with behavioral performance (FWE-corrected $p < 0.001$) for dynamic (blue) and static (red) emotion recognition, identified using a two-tailed, permutation-based maximum statistic approach. A disconnectome analysis for the white matter revealed tracts associated with dynamic (in purple) and static (in yellow) emotion recognition. [AF Arcuate fasciculus, MDLF Middle longitudinal fasciculus, ILF Inferior longitudinal fasciculus, IFOF Inferior fronto-occipital fasciculus].

of lesion-behavior relationships. Unlike ROI methods, SVR-LSM is more data-driven as it does not rely on predefined regions, hence reducing bias and enabling a more comprehensive whole-brain analysis. Using this method, we adjusted for confounding factors such as lesion size, etiology, and time from onset known to affect behavior, thereby enhancing our understanding of the lesion's impact on behavior (see "Methods"). Consistent with our double dissociation findings, we identified a single cluster along the right pSTS that was associated with performance in the dynamic emotion task (Fig. 2). For static emotion recognition, we identified significant bilateral clusters (right > left) over the fusiform and lingual gyrus including the FFA (Fig. 2C) (Table S7). To understand how lesions in one part of the cortex can affect distant regions through their white matter connections, we identified the white matter tracts associated with the behavioral performance on the static and dynamic tasks. To do so, we used the clusters resulting from the SVR-LSM approach as seeds for diffusion tractography. The white matter tracts that exclusively passed through these clusters were identified using a disconnectome analysis approach (see "Methods"). We found that the white matter tracts associated with the dynamic emotion recognition cluster were over the right middle longitudinal fasciculus (MdLF) and over parts of the right arcuate fasciculus (Fig. 2C-purple). For static emotion recognition, we found clusters over the inferior longitudinal fasciculus (ILF) and the inferior fronto-occipital fasciculus (IFOF) (Fig. 2C-yellow). To see if the performance could be determined by brain regions distant but connected to the lesion, we also performed SVR-LSM on indirectly derived functional connectivity maps and disconnectome maps. However, we did not find significant associations beyond the face processing network (see Supp. Info.).

https://doi.org/10.1038/s41467-025-61395-9

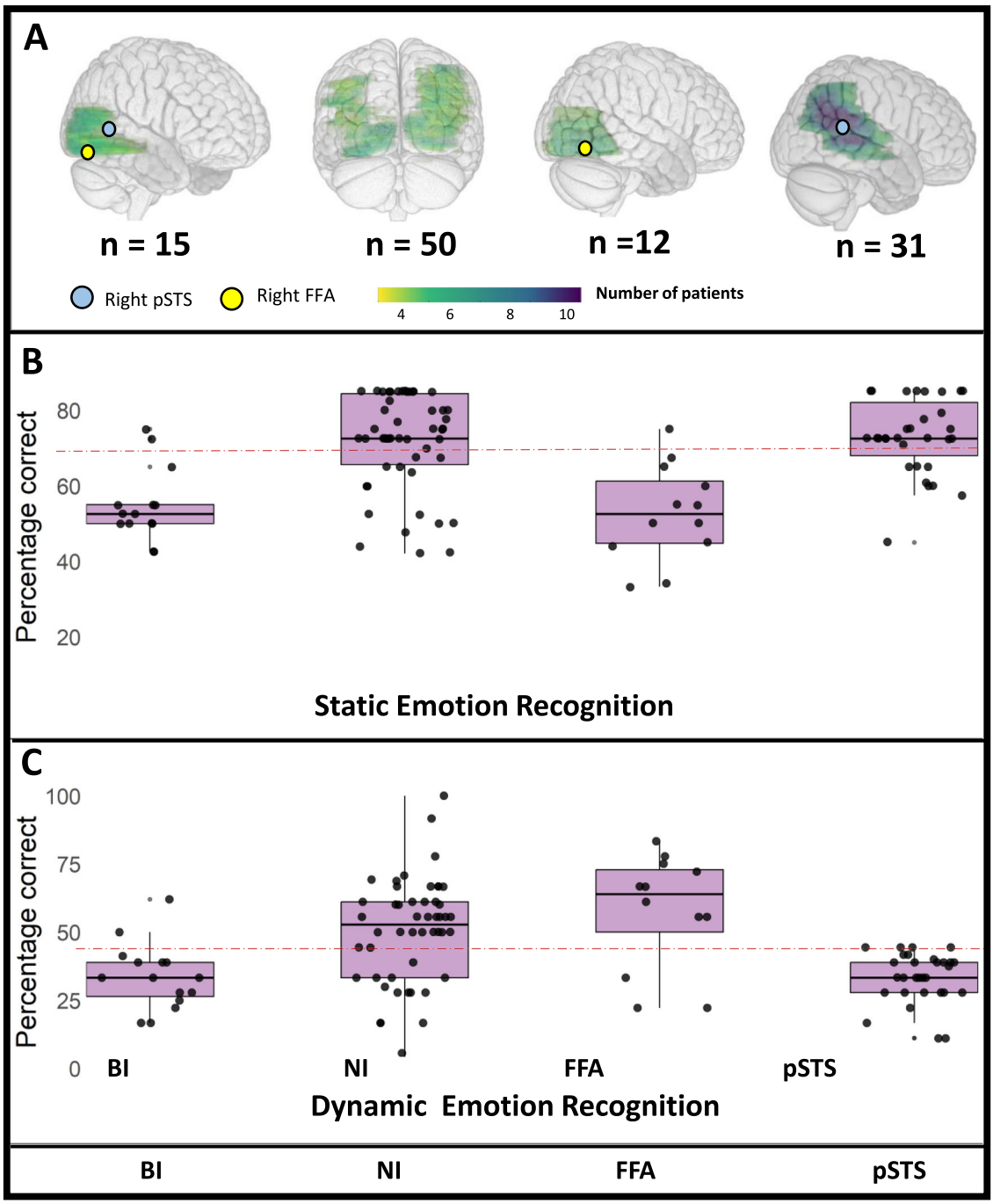

Fig. 3 | ROI analysis comparing static and dynamic emotion recognition based on the right face processing network. Performance on static and dynamic emotion recognition tasks of patients with focal brain lesions to face processing regions in the right hemisphere. Patients were categorized as having isolated lesions involving the right posterior superior temporal sulcus (pSTS) ($N = 31$), isolated lesions of the right fusiform face area (FFA) and occipital face area (OFA) ($N = 12$, FFA), lesions involving both right pSTS and OFA/FFA ($N = 15$, BI), and lesions where neither of these regions were involved ($N = 50$, NI). **A** shows the rendered MNI152 template brain with color-scale denoting the extent of the lesion in each of the categories. **B**, **C** show boxplots for the performance accuracy on the static and dynamic emotion recognition tasks categorized by lesion location. The boxes denote the interquartile range, the whiskers extend to 1.5 × IQR from each quartile and the horizontal lines denote the median. The dots denote individual patient's performance. There is a double dissociation between the right FFA/OFA lesions and right pSTS with regards to static and dynamic emotion recognition, respectively. BI - Lesions involving both right FFA/OFA and pSTS, NI- Lesions not involving both right FFA/OFA and pSTS, FFA- lesions involving the right FFA/OFA, pSTS- lesions involving the right posterior superior temporal sulcus. Red dotted line denotes cut-off threshold for the performance accuracy derived from normative data (shown in Table S3). The source data and code used for generating the plots are available at https://osf.io/ez9dp/.

Discussion

In this study, we provide causal evidence for the putative third visual pathway. We demonstrate this with converging behavioural and neuroimaging evidence for a double dissociation for static and dynamic face reception in ($N = 108$) patients with focal lesions. Classic models of face perception posited that the OFA (a cluster along the ventral stream in the inferior occipital gyrus (IOG), also known as IOG-faces) was the initial entry point for face processing, relaying information to

https://doi.org/10.1038/s41467-025-61395-9

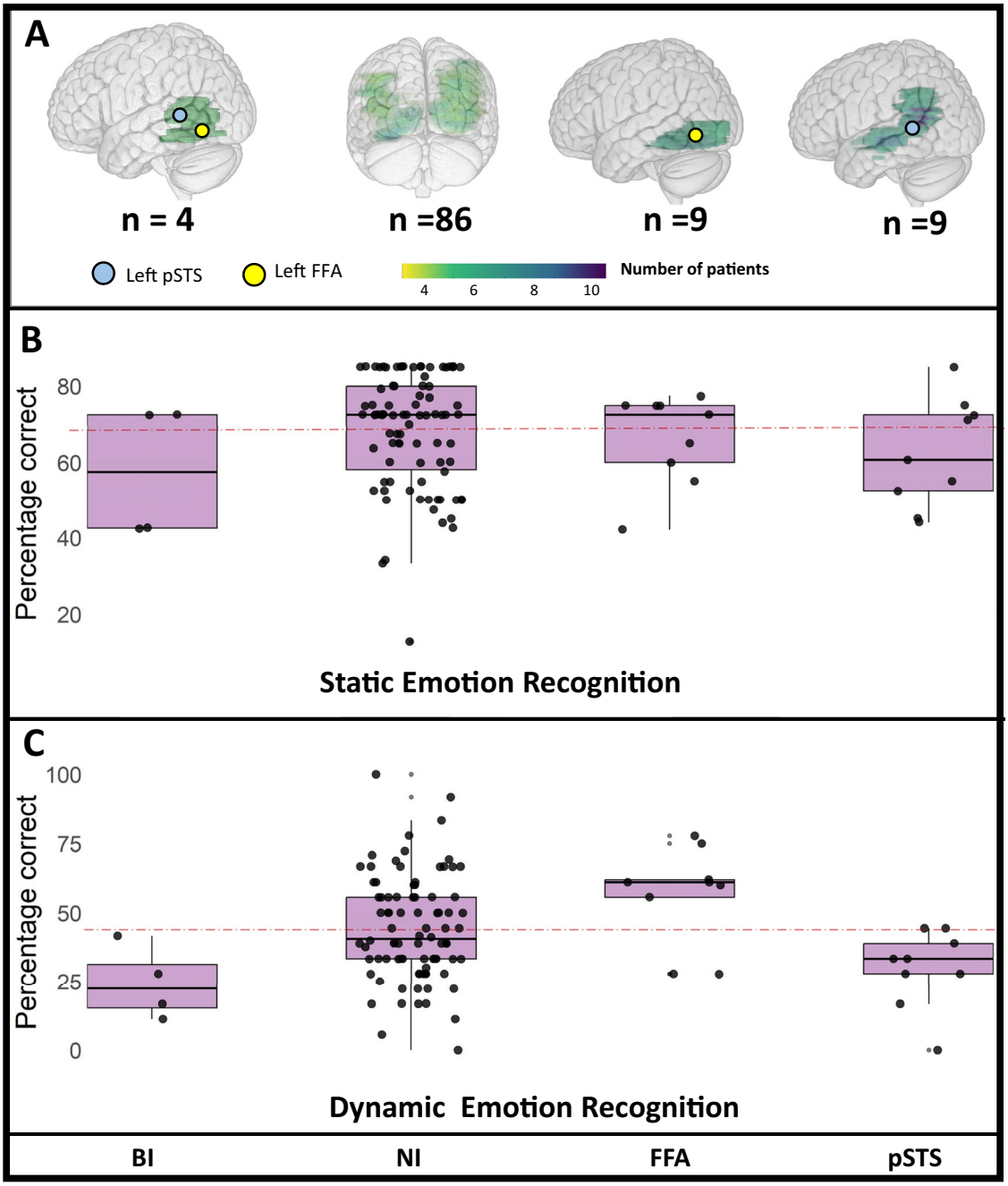

Fig. 4 | ROI analysis comparing static and dynamic emotion recognition based on the left face processing network. Performance on static and dynamic emotion recognition tasks of patients with focal brain lesions to face processing regions in the left hemisphere. Patients were categorized as having isolated lesions involving the left posterior superior temporal sulcus (pSTS) ($N = 9$), isolated lesions of the right fusiform face area (FFA) and occipital face area (OFA) ($N = 9$, FFA), lesions involving both right pSTS and OFA/FFA ($N = 4$, BI), and lesions where neither of these regions were involved ($N = 86$, NI). **A** shows the rendered MNI152 template brain with color-scale denoting the extent of the lesion in each of the categories. **B**, **C** boxplots show the performance accuracy of the static and dynamic emotion recognition tasks categorized by lesion location. The boxes denote the inter-quartile range, the whiskers extend to 1.5 × IQR from each quartile and the horizontal lines denote the median. Left pSTS lesions were associated with poor performance on the dynamic emotion task, while left FFA lesions had normal performance on static emotion recognition. **BI**- Lesions involving both left FFA/OFA and pSTS ROIs **NI**- Lesions not involving both left FFA/OFA and pSTS, **FFA**- lesions involving left FFA/OFA, **pSTS**- lesions involving the left pSTS. Red dotted line denotes cut-off threshold for the performance accuracy derived from normative data (shown in Table S3). The source data and code used for generating the plots are available at https://osf.io/ez9dp/.

the FFA and pSTS[2,24]. While direct connections of OFA to the FFA have been demonstrated, its inputs to the pSTS have not yet been established[3,13–16,20]. Additionally, patients with lesions in the right OFA and right FFA still exhibit normal face-selectivity in the right posterior superior temporal sulcus-face area (pSTS-FA), leading to revisions of these models[5,25,26]. Current models propose that dynamic faces are processed via a parallel pathway that runs from early visual cortex into the pSTS, via the Middle temporal area (hMT+), a key brain region associated with motion processing, bypassing the OFA and FFA[3,7,14,16,27]. According to these models, the primary functional division between the dorsal and ventral pathways of the face perception network lies in the dissociation of motion and form information[3,16]. They suggest that

https://doi.org/10.1038/s41467-025-61395-9

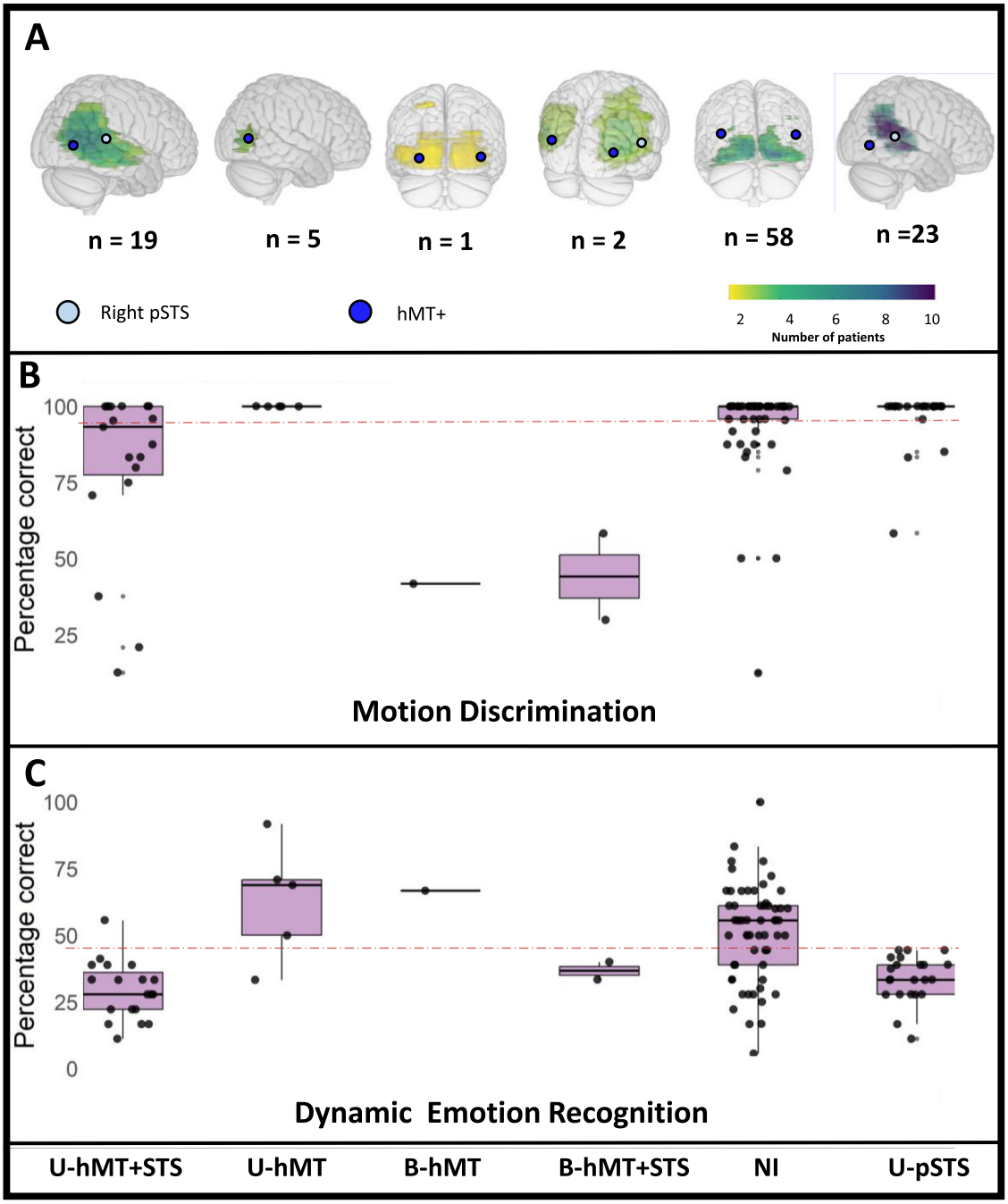

Fig. 5 | ROI analysis comparing motion direction discrimination and dynamic emotion recognition based on the lesion extending to STS and hMT+. Performance on motion direction discrimination and dynamic emotion recognition tasks of patients with focal brain lesions. Patients were categorized as: isolated unilateral posterior superior temporal sulcus (pSTS) lesions ($N = 23$), isolated unilateral motion selective human middle temporal area (hMT+) lesions ($N = 5$), bilateral hMT + lesions ($N = 1$), bilateral hMT+ lesions with pSTS involvement ($N = 2$), unilateral hMT+ and pSTS involvement ($N = 19$), and no involvement of pSTS or hMT+ ($N = 58$). **A** shows the rendered MNI152 template brain with color-scale denoted the extent of the lesion in each of the categories. **B**, **C** boxplots show the performance accuracy of the motion direction discrimination and dynamic emotion recognition tasks categorized by lesion location. The boxes denote the interquartile range, the whiskers extend to 1.5 × IQR from each quartile and the horizontal lines denote the median. Each of the dots denotes individual patient's performance. Patients with bilateral hMT+ lesions had normal performance on dynamic emotion recognition but impaired motion direction recognition. **U-hMT + STS** – Unilateral involvement of hMT+ and pSTS, **U-hMT**- Unilateral involvement of hMT+, **B-hMT** – Bilateral involvement of hMT+, **B-hMT + STS**- involvement of bilateral hMT+ and pSTS on at least one side, **NI** – Both not involved, **U-pSTS**- Unilateral isolated posterior superior temporal sulcus lesions. Red dotted line denotes cut-off threshold for the performance accuracy derived from normative data (Table S3). The source data and code used for generating the plots are available at https://osf.io/ez9dp/.

facial expressions involve both pathways: the ventral pathway extracts form information, while the dorsal pathway processes motion[16]. The pSTS processes dynamic facial information, such as head rotation, eye gaze, and expressions, and may also extract motion-related details from invariant features like identity[2,3,13,15–17,19,28]. Conversely, the FFA, which includes 2 subregions FFA1 and FFA2, primarily extracts form information from static face images, conveying both invariant (identity, race, age) and changeable aspects, including

expressions[2,3,7,16,20,27,29,30]. It has been previously demonstrated in functional neuroimaging studies that the pSTS is selective to dynamic elements of facial expression[8,14,19,20,31,32]. Direct inputs to the pSTS via the motion selective areas hMT+ independent of the ventral OFA and FFA have been demonstrated in both human tractography studies[33] and tracer studies in macaques[34]. While most human lesion studies support the dissociation between face processing networks and the pSTS's role in dynamic facial expression, one study reported a patient with a selective lesion to the right pSTS, showing impaired matching of static facial expressions[20,35–38]. Upon reviewing the lesion image, we noticed that it extended to the right thalamus, particularly the pulvinar, which plays a key role in emotional recognition[38–43]. In our study, lesions involving the pulvinar were associated with impaired performance on all emotion recognition tasks, suggesting that the static emotion recognition impairment in this patient could possibly be due to pulvinar involvement. A TMS study that inhibited the pSTS showed evidence for a double dissociation between dynamic and static emotion recognition[8]. While TMS reveals causal brain-behavior links through temporary disruptions, lesion studies such as ours, uncover the long-term effects of tissue loss and neuroplasticity[44,45]. Together, they provide converging evidence: TMS offers precision and transient insights, while lesions reveal enduring impacts. Double dissociations identified through both methods provide robust causal evidence for the third visual pathway. In our study, by using static facial expressions to study the ventral face processing pathway and dynamic facial expressions to study the dorsal facial pathway, we demonstrated a double dissociation that supports the current face processing model[3,16]. Thus, by showing that the pSTS has inputs independent of the FFA and OFA, we provide causal evidence for (1) the independent role of the pSTS in dynamic face processing and (2) the third visual pathway in humans that bypasses FFA and OFA[3,5,7,8,13,14,19,20].

We also found a double dissociation between motion direction discrimination and dynamic face recognition, thus demonstrating that impairment in dynamic emotion recognition is not part of a global motion perception deficit. Moreover, one patient, with isolated bilateral lesions in the region of hMT+ and sparing of the pSTS, had normal performance in the dynamic emotion recognition task despite impairments in motion direction discrimination. This suggests that there are additional inputs to face selective areas of the pSTS that bypass the cortical motion selective areas (hMT+)[16]. From non-human primate studies, it is known that the pulvinar nucleus has direct projections to the pSTS that bypass the lateral geniculate to V1 pathway[41,46]. We propose that this may be an alternate short-cut in humans, for dynamic facial information from pulvinar to pSTS, bypassing both V1 and hMT+[16].

The face perception network has previously been shown to have a right-hemispheric dominance by multiple methods, including lesion studies and functional MRI[29,47,48] (but see recent evidence challenging this view[49]). Consistent with the traditional view, our ROI analysis, showed that only the right FFA was associated with low scores on the static emotion recognition task. However, lesions to either right or left pSTS were associated with low scores on dynamic emotion recognition. In contrast to this finding, our multivariate SVR-LSM showed a significant cluster only along the right STS for the dynamic emotion recognition. For static emotion, on the other hand, we found bilateral clusters but with right predominance. This finding could probably be explained by the fact that some of the FFA lesions were bilateral due to posterior cerebral artery territory strokes. This co-occurrence of the lesions may have contributed to bilateral clusters in SVR-LSM for static emotion recognition. Our use of SVR-LSM enhances the evidence for the third visual pathway by providing a data-driven, apriori analysis that complements traditional ROI-based methods reliant on predefined regions. The identification of non-overlapping clusters for lesions and white matter disconnection in SVR-LSM reinforces the evidence for a double dissociation between dynamic and static emotion recognition, thus providing convergent evidence for the third visual pathway.

On studying the white matter tracts associated with the ventral visual pathway, consistent with previous studies, we found that the inferior longitudinal fasciculus (ILF) and the inferior fronto-occipital fasciculus (IFOF) were associated with static emotion recognition[6,30]. However, the white matter connections in the putative third pathway for face processing along the superior temporal sulcus continues to be debated[16]. Probabilistic tractography indicates that 70–85% of voxels in this pathway are unclassified, dominated by short association fibers rather than long-range tracts[16,33,50]. Unlisted tracts, including extreme/external capsule and the middle longitudinal fasciculus (MdLF) and the arcuate fasciculus, have been implicated[13,14,16,51]. Our findings show the involvement of the MdLF and arcuate fasciculus in dynamic emotion recognition, with connections extending to the frontal lobe but not to the FFA or OFA support their role in the third visual pathway.

Handedness and sex has been shown to affect lateralization in the face perception network[49]. However, we did not find any association between behavioural scores and sex. Since all our patients were right-handed, we could not study the effect of handedness. As face processing in real life is a complex, yet unified process, the neural pathways that independently contribute to both dynamic and static emotion recognition are likely to contribute the larger face processing network. This overlap in function may be the reason we were not able to predict behavioral performance from functional networks and white matter disconnections beyond the effect of the lesions themselves.

Our study is not without limitations. As behavioural testing was done in hospitalized patients with significant disabilities and often other comorbidities, we limited the overall time of behavioural testing by reducing the number trials per task to a minimum. Moreover, the ROIs used in our study were extracted from the literature, rather than based on individual functional activation. Since these are functionally defined areas, they are likely to vary in anatomical location for each patient. However, considering the large size of the lesions compared to the typical variability in the ROI locations, this limitation is likely to be minimal. The static emotion recognition task using 2D photos is easier than the dynamic task with 3D avatar videos, a difference that could be a limitation. However, the poor performance of FFA lesion patients on the easier static task but normal performance on the dynamic task strengthens the evidence for a double dissociation. The methods of lesion symptom mapping, lesion network mapping, and disconnectome mapping each present specific limitations that affect the interpretation of results. These include challenges related to image resolution variability, the accuracy of lesion segmentation from healthy tissue, the potential distortions introduced by normalization techniques aligning brain images to a standard template, and the complexities of applying statistical corrections for multiple comparisons[22,52,53].

In conclusion, we demonstrate a double dissociation between the perception of dynamic and static facial emotional expressions in a large lesion–symptom mapping study. We provide direct evidence for the third pathway of visual processing, showing that the pSTS has inputs that bypass both the FFA and OFA, playing an important role in the recognition of dynamic facial expressions.

Methods

Subjects

Patients were recruited from the neurological sciences department of the Christian Medical College (CMC) and hospital, Vellore, which is a 2500 bedded quaternary care hospital in south India. Patients with the following diagnoses were initially screened during the study period from January 2022 to January 2023: (1) Acute ischemic strokes within 14 days from the time of onset. (2) Ischemic stroke at least six months from symptom onset with focal gliotic lesion on neuroimaging. (3) Cerebral venous thrombosis with a focal haemorrhage or venous

infarct involving the cerebral cortex. (4) Solitary neurocysticercal lesion involving the cerebral cortex. (5) Benign brain tumour, post excision with focal brain lesion. All patients screened underwent a detailed neurological examination, which included the state of consciousness, screening for ocular cause of visual loss, bed side assessment for visual field defects, hearing loss, aphasia, and focal sensory or motor deficits. Patients were then selected for the study based on the following inclusion criteria: (1) Focal cortical lesions involving the temporal, parietal or occipital lobes, (2) availability of multiplanar MRI brain images showing a clearly identifiable cortical lesion with diffusion weighted imaging (DWI) and/or fluid-attenuated inversion recovery (FLAIR), (3) sufficiently clinically stable to perform behavioural tasks when sitting upright. The exclusion criteria included, (1) impaired or fluctuating level of consciousness, (2) impaired attention, (3) visual impairment due to ocular pathology, (4) hearing loss, (5) impairment in communication/aphasia, (6) patients who are unable to perform psychophysical tasks, (7) diffuse lesions on the MRI, (8) lesions without cortical lesions, and (9) brain lesions where lesion segmentation was not possible. Selected patients who met these criteria and provided informed consent were recruited for the study. A total of 108 participants were included, with a mean age of 45.3 years (SD = 15.3), and 33 (30.6%) were female. For patients who were illiterate or had visual impairments following their stroke, the study details were explained in their native language prior to obtaining informed consent. The study was approved by the Institutional Review Boards of CMC Vellore (IRB min no 2409143) and is in accordance with the Declaration of Helsinki.

Behavioural Tasks

All experiments were coded in PsychoPy version 3.0 and were presented on 1920 × 1080 monitor with 60 Hz refresh rate. The participants were seated at 70 cm from the monitor. The test procedure was first explained to the participant. Testing was binocular and the experimenter watched the patient for saccadic eye movements and lapses of attention. Individual trials with lapses of attention or eye movements were identified and marked by the experimenter and excluded from analysis. Blocks with more than 3 trials with lapses of attention were repeated. The stimuli were displayed until the patient responded verbally, and the experimenter entered the response on the computer keyboard. The patient underwent a battery of tests that assess higher order vision (Table S1). The experimenter was blinded to each patient's lesion location and imaging data while each participant performed the task.

Static facial expressions

To test the ventral pathway of face perception, we selected static emotion recognition over facial identity recognition to isolate face perception from memory influences. Many of our patients had posterior cerebral artery strokes with hippocampal involvement, which could confound identity tasks. This approach enabled a direct comparison with dynamic emotion recognition, differing only by the absence of motion. For the static emotion recognition task, the face images were taken from the Penn Emotion Recognition Task (ER-40)[54]. This contains forty color photographs of faces of different ethnicity, expressing the four basic feelings happy, sad, angry, and fearful, as well as a "no emotion" expression. The stimuli were displayed in the center of the screen such that the size of the image was 10 × 12°. The participants had to choose from the displayed options (5AFC: happy, sad, fearful, angry, or neutral) with a verbal response. For participants who were illiterate, the options were read out in sequence until they chose a response. If no response was made, despite paying attention to the stimuli after 10 s, the trial was terminated by examiner and the next trial was initiated after an interstimulus interval of 500 milliseconds. Normative data from a neurotypical population (N = 68) showed a mean score of 85% and a standard deviation of 7% (Table S3). Based on this distribution, we chose the cutoff threshold of 71% as a performance benchmark, capturing significant deviations from typical performance levels.

Dynamic facial expressions

The face stimuli for the dynamic emotion recognition were created using the FACSHuman plugin for the MakeHuman software[55]. FACSHuman software program, is a tool for creating facial expressions on avatars, based on the Facial Action Coding System (FACS) developed by ref. 56. FACSHuman allows almost all the Action Units (AUs) described in the FACS Manual to be manipulated through a three-dimensional modelling software interface[55]. Using the MakeHuman software, 3 different avatars were built (1 male, 1 female, and 1 gender neutral) and six videos of emotional expressions for happy, sad, anger, surprise, disgust, and fear were created. The videos started with a neutral expression and the defined emotional expression was sequentially ramped up to a maximum of 80% over 1.5 s. The video was generated from 75 individual images that were played at 25 frames per second. The video was played in a loop in the center of the screen such that the size of the image was 10 × 12°. The participants had to choose from the displayed options (6AFC: happy, sad, fearful, angry, surprised, or disgust) with a verbal response. For participants who were illiterate, the options were read out in sequence until they chose a response. If no response was made, despite paying attention to the stimuli after 10 s, the trial was terminated by examiner and the next trial was initiated after an interstimulus interval of 500 milliseconds. Each participant completed one block of 18 trials. Normative data from a neurotypical population (N = 73) showed a mean of 66% and a standard deviation of 11% (Table S3). A cutoff of 44% was set to capture significant deviations from typical performance. Dynamic emotion recognition, especially from facial expressions alone, is a challenging task. Krumbherger et al.'s review of 14 dynamic emotion databases found human performance accuracy at 65.11% (SD = 26.18%) in dynamic emotion recognition, indicating lower performance and cutoff thresholds for dynamic emotions compared to static ones[57].

Motion direction discrimination task

The task involved identifying the global motion direction of a random dot kinematogram (RDK). The stimuli consisted of dynamic random dot displays of 158 white dots (79.2 cd/m^2, subtending 4 arcmin), on a grey background, uniformly distributed within a circular 10° aperture displayed at the centre of the display. The stimuli were generated using the Dots component in PsychoPy and the tests were designed based on a direction discrimination task performed on patients with stroke by ref. 58. Each dot motion sequence lasted 22 frames, after which it was replaced by a new one at a random location. Dot speed was 3°/s and dot density was 2 dots/deg^2. The dot direction was limited to 90, 180, 270, and 360° with 100% coherence and direction of the dots was varied randomly across each trial. The RDK were displayed until key press. The response had to be chosen from the fixed choice of 4 directions (4AFC- Up, down, left, and right). A total of 24 trials were performed by each participant.

Biological motion task

This task involved identification of the actions performed by human participants displayed as point-light displays (PLDs). The stimuli consists of 20 videos of human point-light walkers with single or dyads, performing some activity (e.g., Walking, running, waving goodbye, and two people hugging)[59]. The videos were 3 s long and were played in loop for a maximum of 30 s. The stimuli were displayed to subtend 10° of visual angle. The participants were asked to recognize the activity and give a free verbal response. The response was judged as correct or incorrect by the examiner. Each participant completed one block of 20 trials.

Social perception task

Social perception was assessed using the Yoni task[60]. The Yoni task involves the ability to judge mental states based on verbal and eye gaze cues. The task stimuli consist of a cartoon outline of a face (named "Yoni") and four pictures of objects belonging to a single category (e.g., fruits, chairs) or faces, one in each corner of the computer screen. The stimuli were presented with in 30° of visual angle from the center of the screen. The participants' task is to point to the correct answer (the image to which Yoni is referring), based on a sentence that appears at the top of the screen and available cues[60]. This task assesses cognitive and affective mentalizing ability[60]. For the participants who were unable to read the sentence presented on the screen, the examiner read out the sentence in the appropriate language and confirmed that the patient comprehended the sentence, by asking them to repeat sentence and state its meaning. Once the patient gave a verbal response, the examiner used the mouse click to record the response. Each participant completed one block of 24 trials.

Color naming task

This task involved identifying and naming the color of a circular disc displayed on the center of the screen. The stimuli consisted of 9 common colors identified and named universally across all cultures in the Indian subcontinent. The colors used were black, blue, brown, green, pink, purple, red, yellow, and white. The colored discs were generated using Psychopy and were displayed to subtend 10° of visual angle. A total of 36 trials were performed by each participant. The participant had to choose from the 9 options with a verbal response[61].

Object naming task

This task involved identifying and naming 50 simple outline drawings of objects. The stimuli were drawn with black outline on a white background and displayed in the centre of the screen to a size of 10° × 12 visual angle. This study was designed based on a task by Newcombe et al., who had worked on brain lesion patients[62]. The response was judged as correct or incorrect by the examiner. If no response was made, despite paying attention to the stimuli after 10 s, the trial was terminated by the examiner and the next trial was initiated after an interstimulus interval of 500 milliseconds. If errors were noted on the object naming task, the participant was asked to perform the object matching and shape matching task to evaluate for visual agnosia.

Behavioural data analysis

We calculated accuracy (percentage of correct responses) and response times for each of the experimental conditions separately. The variables were z-transformed, based on the normative values of the respective healthy control groups (Table S3) and D'prime and A'prime were estimated using the R package "psycho"[63].

Neuroanatomical data and analysis

Lesion Mapping. Clinical MRI data was reviewed and T2w, T2FLAIR, T1w, and DWI sequences were used to map the lesions. For acute ischemic stroke DWI sequences were primarily used, while for chronic lesions, T2 FLAIR was used. The lesion was mapped directly onto the Montreal Neurological Institute (MNI) space manually using MRIcroGL (https://www.nitrc.org/projects/mricrogl)[64]. The lesion was mapped in 3D using simultaneous axial, coronal, and sagittal views by the neurologist ATP, who is experienced in lesion mapping and cross verified by an independent neurologist. Edits in the lesion margins were made by consensus[65].

Region of interests (ROI) analysis

The OFA, FFA, and the pSTS were the ROIs included from the face processing network[19]. MNI coordinates of the peak activations to face stimuli, identified on task-based f-MRI from literature were used, and a 6 mm spherical (ROI) was created using the MarsBaR toolbox for SPM[23,66]. The coordinates of the ROIs of the face processing network and the other ROIs of the higher order visual pathway are summarized in Table S2. Each patient's lesion map in MNI space was overlapped with the selected ROIs to study the extent of the lesion to the functionally defined regions. Patients were then categorized into 4 groups as follows: (1) Isolated lesions to the right pSTS. (2) Isolated lesions to right OFA/FFA. (3) Lesions involving both right pSTS and OFA/FFA. (4) Lesions involving neither the right pSTS or right OFA/FFA. A General Linear Model (GLM) was constructed to assess the main effects and interactions. Performance Accuracy on the static and dynamic emotion recognition tasks were included as dependent variables alternately, with each serving as a covariate in turn. The lesion groups were entered as the independent factor. Similar analysis was performed for the face processing regions of the left side and for the ROIs involved in global notion perception, such as hMT + .

Lesion network mapping

Lesion network mapping is a validated technique that identifies regions functionally connected to a lesion location, allowing one to localize symptoms even when lesions occur in different brain locations using the normative connectome data[52]. An open source normative resting state−fMRI dataset assembled from the 1000 healthy Brain Genomics Superstruct Project (https://dataverse.harvard.edu/dataverse/GSP) was used for lesion network mapping[67]. Processing of the resting state fMRI data was performed with SPM-12 (Wellcome Department of Imaging Neuroscience, London, UK) and the CONN functional connectivity toolbox[68] both implemented in Matlab R2022a (The Math Works, Natick, MA, USA). The manually drawn lesion map was used as a seed in a resting state functional connectivity MRI analysis using the CONN toolbox. A connectivity r-map thus obtained for the lesion was converted to t-maps and thresholded at $T > \pm 5$ to create a map of significantly functionally connected regions to the patient's lesion site (whole-brain voxel-wise FWE-corrected $p < 0.05$)[52]. The thresholded but non-binarized lesion maps were used in a multivariate lesion network symptom mapping method using SVR LSM to identify the networks that were associated with the behavioural score of interest.

Lesion disconnectome mapping

For each patient's lesion map, the disconnected white matter tracts were estimated as disconnectome maps using the BCBtoolkit[53]. The lesion maps in MNI space was used as a seed region for tractography to identify the white matter fibers that are anatomically connected to the lesion[53]. The resulting disconnectome map, which denotes the probability of disconnection from 0 to 100% for each voxel in the brain was used in a multivariate lesion network symptom mapping method using SVR LSM to identify the damaged white matter pathways that were associated with the behavioural score of interest.

Multivariate lesion–symptom mapping using support vector regression

For each behavioural measure of interest, support vector regression-based multivariate lesion–symptom mapping analysis (SVR-LSM) was performed on the lesion maps, lesion networks, and disconnectomes separately. The advantage of using this method in comparison to the traditional univariate voxel-based lesion–symptom mapping analysis was that, it can adjust for intervoxel correlations, lesion volume, and identify multivariate interactions between lesion location and studied symptoms[50]. Lesions in stroke and tumors can often be treated as binary variables, where tissue is either completely damaged or intact. However, functional and structural connectivity measures, such as brain network connectivity or white matter integrity, typically represent continuous variables, reflecting a range of values rather than just two categories. Binarizing these continuous measures can lead to the

loss of valuable information about the varying degrees of connectivity across different regions of the brain. To preserve this information, we used non-binarized maps for lesion network mapping and disconnectome mapping. This approach allows for the retention of the full spectrum of structural and functional connectivity values across the brain. By maintaining continuous data, we avoid oversimplifying the complexity of brain connectivity. Initial SVR-LSM was conducted using the SVR lesion symptom mapping toolbox (https://github.com/atdemarco/svrlsmgui) with functionalities of the Statistics and Machine Learning Toolbox within MATLAB (MATLAB 2022a, The MathWorks, Inc., Natick, Massachusetts, United States)[50,69]. The SVR analysis was restricted to voxels with at least ten overlapping lesions using a radial basis function kernel with default hyperparameters of gamma = 5 and cost = 30[69,70]. To validate the approach, we repeated the SVR-LSM method using an in-house Python pipeline with grid search and *K*-fold cross-validation to optimize hyperparameters. This implementation identified Epsilon = 0.1, Cost = 10, gamma = 2, at $K = 5$ as optimal values. (The code used for this analysis is available at https://doi.org/10.5281/zenodo.15280654)[71]. Lesion volume was regressed out of both, behavioural data and lesion maps. The type of lesion (acute/chronic) and other behavioural scores showing significant correlation with the behavioural score of interest were added as covariates. The resultant raw regression β values were thresholded at $p < 0.005$ and corrected for cluster size at $p < 0.05$, both based on 10,000 permutations. Anatomical location of all clusters was determined according to the Harvard–Oxford Cortical, Automated Anatomical Labelling atlas 3 (AAL3) and the Juelich Atlas[72,73]. The IIT atlas was used to identify the possible white matter tracts damaged by the lesion[74].

Reporting summary

Further information on research design is available in the Nature Portfolio Reporting Summary linked to this article.

Data availability

Anonymized behavioral data is available on OSF at https://osf.io/t6e9h, and lesion files will be provided on request, adhering to patient privacy guidelines.

Code availability

The code used in this analysis is available on OSF at https://osf.io/ez9dp/.

References

1. Mishkin, M., Ungerleider, L. G. & Macko, K. A. Object vision and spatial vision: two cortical pathways. *Trends Neurosci.* **6**, 414–417 (1983).
2. Calder, A. J. & Young, A. W. Understanding the recognition of facial identity and facial expression. *Nat. Rev. Neurosci.* **6**, 641–651 (2005).
3. Duchaine, B. & Yovel, G. A revised neural framework for face processing. *Annu. Rev. Vis. Sci.* **1**, 393–416 (2015).
4. Haxby, J. V., Hoffman, E. A. & Gobbini, M. I. The distributed human neural system for face perception. Trends Cogn. Sci. 4, 223–223 (2000).
5. Steeves, J. K. E. et al. The fusiform face area is not sufficient for face recognition: evidence from a patient with dense prosopagnosia and no occipital face area. *Neuropsychologia* **44**, 594–609 (2006).
6. Tavor, I. et al. Separate parts of occipito-temporal white matter fibers are associated with recognition of faces and places. *NeuroImage* **86**, 123–130 (2014).
7. O'Toole, A. J., Roark, D. A. & Abdi, H. Recognizing moving faces: a psychological and neural synthesis. *Trends Cogn. Sci.* **6**, 261–266 (2002).
8. Pitcher, D., Dilks, D. D., Saxe, R. R., Triantafyllou, C. & Kanwisher, N. Differential selectivity for dynamic versus static information in face-selective cortical regions. *Neuroimage* **56**, 2356–2363 (2011).
9. Dumoulin, S. O., Baker, C. L., Hess, R. F. & Evans, A. C. Cortical specialization for processing first- and second-order motion. *Cereb. Cortex* **13**, 1375–1385 (2003).
10. Larsson, J. & Heeger, D. J. Two retinotopic visual areas in human lateral occipital cortex. *J. Neurosci.* **26**, 13128–13142 (2006).
11. Gomez, J. et al. Development of population receptive fields in the lateral visual stream improves spatial coding amid stable structural-functional coupling. *Neuroimage* **188**, 59–69 (2019).
12. Seltzer, B. & Pandya, D. N. Afferent cortical connections and architectonics of the superior temporal sulcus and surrounding cortex in the rhesus monkey. *Brain Res.* **149**, 1–24 (1978).
13. Pitcher, D. et al. The human posterior superior temporal sulcus samples visual space differently from other face-selective regions. *Cereb. Cortex* **30**, 778–785 (2020).
14. Pitcher, D. & Ungerleider, L. G. Evidence for a third visual pathway specialized for social perception. *Trends Cogn. Sci.* **25**, 100–110 (2021).
15. Weiner, K. S. & Gomez, J. Third visual pathway, anatomy, and cognition across species. *Trends Cogn. Sci.* **25**, 548–549 (2021).
16. Puce, A. From motion to emotion: visual pathways and potential interconnections. *J. Cogn. Neurosci.* 1–24 https://doi.org/10.1162/jocn_a_02141 (2024).
17. Weiner, K. S. & Grill-Spector, K. Neural representations of faces and limbs neighbor in human high-level visual cortex: evidence for a new organization principle. *Psychol. Res.* **77**, 74–97 (2013).
18. Candidi, M., Stienen, B. M. C., Aglioti, S. M. & de Gelder, B. Virtual lesion of right posterior superior temporal sulcus modulates conscious visual perception of fearful expressions in faces and bodies. *Cortex* **65**, 184–194 (2015).
19. Pitcher, D., Duchaine, B. & Walsh, V. Combined TMS and fMRI reveal dissociable cortical pathways for dynamic and static face perception. *Curr. Biol.* **24**, 2066–2070 (2014).
20. Sliwinska, M. W., Bearpark, C., Corkhill, J., McPhillips, A. & Pitcher, D. Dissociable pathways for moving and static face perception begin in early visual cortex: evidence from an acquired prosopagnosic. *Cortex* **130**, 327–339 (2020).
21. Bauer, R. M. Autonomic recognition of names and faces in prosopagnosia: a neuropsychological application of the guilty knowledge test. *Neuropsychologia* **22**, 457–469 (1984).
22. Vaidya, A. R., Pujara, M. S., Petrides, M., Murray, E. A. & Fellows, L. K. Lesion studies in contemporary neuroscience. *Trends Cogn. Sci.* **23**, 653–671 (2019).
23. Schobert, A.-K., Corradi-Dell'Acqua, C., Frühholz, S., van der Zwaag, W. & Vuilleumier, P. Functional organization of face processing in the human superior temporal sulcus: a 7T high-resolution fMRI study. *Soc. Cogn. Affect. Neurosci.* **13**, 102–113 (2018).
24. Bruce, V. & Young, A. Understanding face recognition. *Br. J. Psychol.* **77**, 305–327 (1986).
25. Rossion, B. et al. A network of occipito-temporal face-sensitive areas besides the right middle fusiform gyrus is necessary for normal face processing. *Brain* **126**, 2381–2395 (2003).
26. Dalrymple, K. A. et al. The anatomic basis of the right face-selective N170 IN acquired prosopagnosia: a combined ERP/fMRI study. *Neuropsychologia* **49**, 2553–2563 (2011).
27. Grill-Spector, K., Weiner, K. S., Kay, K. & Gomez, J. The functional neuroanatomy of human face perception. *Annu. Rev. Vis. Sci.* **3**, 167–196 (2017).
28. Allison, T., Puce, A. & McCarthy, G. Social perception from visual cues: role of the STS region. *Trends Cogn. Sci.* **4**, 267–278 (2000).
29. Barton, J. J. S. Structure and function in acquired prosopagnosia: lessons from a series of 10 patients with brain damage. *J. Neuropsychol.* **2**, 197–225 (2008).
30. Gomez, J. et al. Functionally defined white matter reveals segregated pathways in human ventral temporal cortex associated with category-specific processing. *Neuron* **85**, 216–227 (2015).

31. Puce, A., Allison, T., Asgari, M., Gore, J. C. & McCarthy, G. Differential sensitivity of human visual cortex to faces, letterstrings, and textures: a functional magnetic resonance imaging study. *J. Neurosci.* **16**, 5205–5215 (1996).
32. Schultz, J. & Pilz, K. S. Natural facial motion enhances cortical responses to faces. *Exp. Brain Res.* **194**, 465–475 (2009).
33. Gschwind, M., Pourtois, G., Schwartz, S., Van De Ville, D. & Vuilleumier, P. White-matter connectivity between face-responsive regions in the human brain. *Cereb. Cortex* **22**, 1564–1576 (2012).
34. Ungerleider, L. G. & Desimone, R. Cortical connections of visual area MT in the macaque. *J. Comp. Neurol.* **248**, 190–222 (1986).
35. Richoz, A.-R., Jack, R. E., Garrod, O. G. B., Schyns, P. G. & Caldara, R. Reconstructing dynamic mental models of facial expressions in prosopagnosia reveals distinct representations for identity and expression. *Cortex* **65**, 50–64 (2015).
36. Cohen, A. L. et al. Looking beyond the face area: lesion network mapping of prosopagnosia. *Brain* **142**, 3975–3990 (2019).
37. Sorger, B., Goebel, R., Schiltz, C. & Rossion, B. Understanding the functional neuroanatomy of acquired prosopagnosia. *Neuroimage* **35**, 836–852 (2007).
38. Fox, C. J., Hanif, H. M., Iaria, G., Duchaine, B. C. & Barton, J. J. S. Perceptual and anatomic patterns of selective deficits in facial identity and expression processing. *Neuropsychologia* **49**, 3188–3200 (2011).
39. Bertini, C., Pietrelli, M., Braghittoni, D. & Làdavas, E. Pulvinar lesions disrupt fear-related implicit visual processing in hemianopic patients. Front. Psychol. 9, 2329 (2018).
40. Maior, R. S., Hori, E., Tomaz, C., Ono, T. & Nishijo, H. The monkey pulvinar neurons differentially respond to emotional expressions of human faces. *Behav. Brain Res.* **215**, 129–135 (2010).
41. Kaas, J. H. & Lyon, D. C. Pulvinar contributions to the dorsal and ventral streams of visual processing in primates. *Brain Res. Rev.* **55**, 285–296 (2007).
42. McFadyen, J., Mattingley, J. B. & Garrido, M. I. An afferent white matter pathway from the pulvinar to the amygdala facilitates fear recognition. *eLife* **8**, e40766 (2019).
43. de Gelder, B., Vroomen, J., Pourtois, G. & Weiskrantz, L. Non-conscious recognition of affect in the absence of striate cortex. Neuroreport 10, 3759–3763 (1999).
44. Joutsa, J., Lipsman, N., Horn, A., Cosgrove, G. R. & Fox, M. D. The return of the lesion for localization and therapy. *Brain* **146**, 3146–3155 (2023).
45. Sliwinska, M. W., Vitello, S. & Devlin, J. T. Transcranial magnetic stimulation for investigating causal brain-behavioral relationships and their time course. *J. Vis. Exp.* 51735 https://doi.org/10.3791/51735 (2014).
46. Yeterian, E. H. & Pandya, D. N. Thalamic connections of the cortex of the superior temporal sulcus in the rhesus monkey. *J. Comp. Neurol.* **282**, 80–97 (1989).
47. Bukowski, H., Dricot, L., Hanseeuw, B. & Rossion, B. Cerebral lateralization of face-sensitive areas in left-handers: only the FFA does not get it right. *Cortex* **49**, 2583–2589 (2013).
48. Thomas, C. et al. Reduced structural connectivity in ventral visual cortex in congenital prosopagnosia. *Nat. Neurosci.* **12**, 29–31 (2009).
49. Thome, I. et al. Let's face it: the lateralization of the face perception network as measured with fMRI is not clearly right dominant. *NeuroImage* **263**, 119587 (2022).
50. Zhang, Y., Kimberg, D. Y., Coslett, H. B., Schwartz, M. F. & Wang, Z. Support vector regression based multivariate lesion-symptom mapping. *Annu. Int. Conf. IEEE Eng. Med. Biol. Soc.* **2014**, 5599–5602 (2014).
51. Wang, Y., Metoki, A., Alm, K. H. & Olson, I. R. White matter pathways and social cognition. *Neurosci. Biobehav. Rev.* **90**, 350–370 (2018).
52. Boes, A. D. et al. Network localization of neurological symptoms from focal brain lesions. *Brain* **138**, 3061–3075 (2015).
53. Foulon, C. et al. Advanced lesion symptom mapping analyses and implementation as BCBtoolkit. Gigascience 7, 1–17 (2018).
54. Pinkham, A. E. et al. The other-race effect in face processing among African American and caucasian individuals with schizophrenia. *AJP* **165**, 639–645 (2008).
55. Gilbert, M., Demarchi, S. & Urdapilleta, I. FACSHuman, a software program for creating experimental material by modeling 3D facial expressions. *Behav. Res.* **53**, 2252–2272 (2021).
56. Ekman, P., Hager, J. C. & Friesen, W. V. *Facial Action Coding System: The Manual* (Research Nexus, Salt Lake City, 2002).
57. Krumhuber, E. G., Küster, D., Namba, S. & Skora, L. Human and machine validation of 14 databases of dynamic facial expressions. *Behav. Res.* **53**, 686–701 (2021).
58. Vaina, L. M. et al. Functional and anatomical profile of visual motion impairments in stroke patients correlate with fMRI in normal subjects. *J. Neuropsychol.* **4**, 121–145 (2010).
59. Decatoire, A. et al. PLAViMoP: how to standardize and simplify the use of point-light displays. *Behav. Res. Methods* **51**, 2573–2596 (2019).
60. Shamay-Tsoory, S. G. & Aharon-Peretz, J. Dissociable prefrontal networks for cognitive and affective theory of mind: a lesion study. *Neuropsychologia* **45**, 3054–3067 (2007).
61. Siuda-Krzywicka, K. et al. Color categorization independent of color naming. *Cell Rep.* **28**, 2471–2479.e5 (2019).
62. Newcombe, F., Oldfield, R. C., Ratcliff, G. G. & Wingfield, A. Recognition and naming of object-drawings by men with focal brain wounds. *J. Neurol. Neurosurg. Psychiatry* **34**, 329–340 (1971).
63. Makowski, D. The psycho package: an efficient and publishing-oriented workflow for psychological science. *J. Open Source Softw.* **3**, 470 (2018).
64. Rorden, C., Karnath, H.-O. & Bonilha, L. Improving lesion-symptom mapping. *J. Cogn. Neurosci.* **19**, 1081–1088 (2007).
65. Rorden, C. & Brett, M. Stereotaxic display of brain lesions. *Behav. Neurol.* **12**, 191–200 (2000).
66. MarsBaR region of interest toolbox for SPM — MarsBaR 0.45 documentation. https://marsbar-toolbox.github.io/.
67. Buckner, R. L., Roffman, J. L. & Smoller, J. W. *Brain Genomics Superstruct Project (GSP)*. https://doi.org/10.7910/DVN/25833 (Harvard Dataverse, 2020).
68. Whitfield-Gabrieli, S. & Nieto-Castanon, A. Conn: a functional connectivity toolbox for correlated and anticorrelated brain networks. *Brain Connect.* **2**, 125–141 (2012).
69. DeMarco, A. T. & Turkeltaub, P. E. A multivariate lesion symptom mapping toolbox and examination of lesion-volume biases and correction methods in lesion-symptom mapping. *Hum. Brain Mapp.* **39**, 4169–4182 (2018).
70. Sperber, C., Wiesen, D. & Karnath, H. An empirical evaluation of multivariate lesion behaviour mapping using support vector regression. *Hum. Brain Mapp.* **40**, 1381–1390 (2018).
71. Cognitive Neuroscience and Clinical phenomenology Lab & rohan3412. cogneuro-rgb/svrLSMpy: svrlsmpy. Zenodo https://doi.org/10.5281/zenodo.15280655 (2025).
72. Desikan, R. S. et al. An automated labeling system for subdividing the human cerebral cortex on MRI scans into gyral based regions of interest. *NeuroImage* **31**, 968–980 (2006).
73. Amunts, K., Mohlberg, H., Bludau, S. & Zilles, K. Julich-Brain: a 3D probabilistic atlas of the human brain's cytoarchitecture. *Science* **369**, 988–992 (2020).
74. Qi, X. & Arfanakis, K. Regionconnect: rapidly extracting standardized brain connectivity information in voxel-wise neuroimaging studies. *Neuroimage* **225**, 117462 (2021).

Acknowledgements

We thank Prof. Trichur Vidyasagar for his review of the data and manuscript. We acknowledge Rohan Thomas Jepagnanam for his contribution

to developing the SVR-LSM Python code. We also extend our gratitude to all our patients for their participation in this study. Funding: University of Melbourne PhD scholarship.

Author contributions

Conceptualization: A.T.P. Methodology: A.T.P., A.R., K.M. Investigation: A.T.P., A.R., K.M. Visualization: A.T.P., A.M.K., O.C., M.G. Funding acquisition: A.T.P. Project administration: A.T.P. Supervision: A.M.K., OC, M.G. Writing–original draft: A.T.P. Writing–review & editing: A.T.P., A.M.K., O.C., M.G.

Competing interests

The authors declare no competing interests.

Additional information

Supplementary information The online version contains supplementary material available at https://doi.org/10.1038/s41467-025-61395-9.

Correspondence and requests for materials should be addressed to A. T. Prabhakar.

Peer review information *Nature Communications* thanks David Pitcher and the other, anonymous, reviewer(s) for their contribution to the peer review of this work. A peer review file is available.